ISSN 1674-1056
http://cpb.iphy.ac.cn
http://iopscience.iop.org/cpb
中国物理 B
Chinese Physics
中国物理 Chinese Physics B

Magnetism and piezoelectricity of hexagonal boron nitride with triangular vacancy

Lu-Si Zhao(赵路丝), Chun-Ping Chen(陈春平), Lin-Lin Liu(刘林林), Hong-Xia Yu(于洪侠), Yi Chen(陈怡), Xiao-Chun Wang(王晓春)
Citation: Chin. Phys. B . 2018, 27(1): 016301. **doi:** 10.1088/1674-1056/27/1/016301

Journal homepage: http://cpb.iphy.ac.cn; http://iopscience.iop.org/cpb

What follows is a list of articles you may be interested in

First-principles analysis of the structural, electronic, and elastic properties of cubic organic-inorganic perovskite $HC(NH_2)_2PbI_3$

Jun-Fei Wang(王俊斐), Xiao-Nan Fu(富笑男), Jun-Tao Wang(王俊涛)
Chin. Phys. B . 2017, 26(10): 106301. **doi:** 10.1088/1674-1056/26/10/106301

First-principles investigations on the mechanical, thermal,electronic, and optical properties of the defect perovskites Cs_2SnX_6 (X= Cl, Br, I)

Hai-Ming Huang(黄海铭), Zhen-Yi Jiang(姜振益), Shi-Jun Luo(罗时军)
Chin. Phys. B . 2017, 26(9): 096301. **doi:** 10.1088/1674-1056/26/9/096301

Structural, electronic, and magnetic behaviors of 5d transition metal atom substituted divacancy graphene: A first-principles study

Rafique Muhammad, Yong Shuai(帅永), He-Ping Tan, Hassan Muhammad
Chin. Phys. B . 2017, 26(5): 056301. **doi:** 10.1088/1674-1056/26/5/056301

The electronic, optical, and thermodynamical properties of tetragonal, monoclinic, and orthorhombic M_3N_4 (M=Si, Ge, Sn): A first-principles study

Dong Chen(陈东), Ke Cheng(程科), Bei-Ying Qi(齐蓓影)
Chin. Phys. B . 2017, 26(4): 046303. **doi:** 10.1088/1674-1056/26/4/046303

Structural, elastic, electronic, and thermodynamic properties of MgAgSb investigated by density functional theory

Jun-Fei Wang(王俊斐), Xiao-Nan Fu(富笑男), Xiao-Dong Zhang(张小东), Jun-Tao Wang(王俊涛), Xiao-Dong Li(李晓东), Zhen-Yi Jiang(姜振益)
Chin. Phys. B . 2016, 25(8): 086302. **doi:** 10.1088/1674-1056/25/8/086302

Magnetism and piezoelectricity of hexagonal boron nitride with triangular vacancy*

Lu-Si Zhao(赵路丝)[1,2], Chun-Ping Chen(陈春平)[1,2], Lin-Lin Liu(刘林林)[1,2], Hong-Xia Yu(于洪侠)[1,2], Yi Chen(陈怡)[1,2], and Xiao-Chun Wang(王晓春)[1,2,†]

[1] *Institute of Atomic and Molecular Physics, Jilin University, Changchun* 130012, *China*

[2] *Jilin Provincial Key Laboratory of Applied Atomic and Molecular Spectroscopy (Jilin University), Changchun* 130012, *China*

(Received 12 October 2017; revised manuscript received 16 November 2017; published online 22 December 2017)

First-principle calculations reveal that the configuration system of hexagonal boron nitride (h-BN) monolayer with triangular vacancy can induce obvious magnetism, contrary to that of the nonmagnetic pristine boron nitride monolayer. Interestingly, the h-BN with boron atom vacancy (V_B-BN) displays metallic behavior with a total magnetic moment being $0.46\mu_B$ per cell, while the h-BN with nitrogen atom vacancy (V_N-BN) presents a half-metallic characteristic with a total magnetic moment being $1.0\mu_B$ per cell. Remarkably, piezoelectric stress coefficient e_{11} of the V_N-BN is about 1.5 times larger than that of pristine h-BN. Furthermore, piezoelectric strain coefficient d_{11} (12.42 pm/V) of the V_N-BN is 20 times larger than that of pristine h-BN and also one order of magnitude larger than the value for the h-MoS_2 monolayer, which is mainly due to the spin-down electronic state in the V_N-BN system. Our study demonstrates that the nitrogen atom vacancies can be an efficient route to tailoring the magnetic and piezoelectric properties of h-BN monolayer, which have promising performances for potential applications in nano-electromechanical systems (NEMS) and nanoscale electronics devices.

Keywords: first-principle, magnetism, piezoelectric, nano-electromechanical systems

PACS: 63.20.dk, 75.70.Ak, 77.65.Ly, 85.85.+j **DOI:** 10.1088/1674-1056/27/1/016301

1. Introduction

The successful synthesis of atomically thick graphene.[1] has triggered enormous interest in research on low-dimensional nanomaterials due to its exciting unusual properties and promising applications in material science. Consequently, hexagonal boron nitride (h-BN) monolayer, a two-dimensional material with the same honeycomb structure as graphene, exhibits completely different physical properties from graphene[2–4] and has been brought to the forefront of research.[5–11] The advances in experimental synthesis of h-BN sheet have led us to explore the properties of h-BN sheet by decorating its surface. High-resolution transmission electron microscopy studies have revealed that the defects in h-BN sheets are primarily triangle-shaped vacancy defects caused during the fabrication of h-BN.[12]

Actually, the structural and electronic properties,[13,14] chemical reactivity[15] and molecular adsorption and dissociation behaviors[16,17] of vacancy-decorated h-BN have been reported. In the pristine h-BN sheet, the charge transfer from B to N atoms and the orbital hybridization make electrons paired and thus the system is nonmagnetic.[18] Interestingly, the vacancies in the h-BN sheet can induce interesting magnetic properties.[19–21] However, how the magnetic property of h-BN sheet changes by increasing the density of the vacancies and considering the interaction between the neighboring vacancies is still an unsolved problem.

The rapidly growing demand for nano-electromechanical systems (NEMS) and nanoscale electronics devices calls for nanoscale piezoelectric materials, promoting investigations into low-dimensional materials.[22–24] For a crystal to be piezoelectric, it must have no center of inversion symmetry.[25] Graphene lacks any intrinsic piezoelectricity due to its symmetry inversion center. None of many two-dimensional (2D) monolayer structures exhibits an inversion symmetry, and thus all of them are intrinsically piezoelectric.[26–29] The most prominent 2D structures are hexagonal boron nitride (h-BN) and some transition metal dichalcogenides (TMDCS) due to their large piezoelectric coefficients.[26,28,29] Interestingly, it was found that that the modified h-BN or h-AlN sheet by hydrogen and/or fluorine also shows an enhanced piezoelectric performance by first-principles calculation.[30,31] The *ab initio* calculations indicate that the emergence of piezoelectricity in g-C_3N_4 is due to the fact that a stable phase of graphene nitride nanosheet is riddled with regularly spaced triangular holes.[32] We predict that the h-BN sheet with triangle-shaped holes may improve piezoelectric performance. Electronic and magnetic properties of h-BN monolayer with mono-vacancy defects have been reported frequently.[13,20,21,33] However, so far, magnetic and piezoelectric properties of h-BN riddled with triangle-shaped holes have not been systematically investigated yet.

Here, we use first-principle calculation to investigate

*Project supported by the National Natural Science Foundation of China (Grant No. 11474123) and the Natural Science Foundation of Jilin Province, China (Grant No. 20170101154JC).

†Corresponding author. E-mail: wangxiaochun@jlu.edu.cn

© 2018 Chinese Physical Society and IOP Publishing Ltd

the magnetic and piezoelectric properties of the vacancy-decorated h-BN monolayer with an array of densest vacancies which have noncentrosymmetric triangular holes in structure. These decorated structures include V_B-BN and V_N-BN, which indicate the h-BN monolayer with one boron atom and one nitrogen atom vacancy decorated in one super cell, respectively. These h-BN monolayer systems with different triangle-shaped vacancies could potentially introduce new functionalities through cross-coupling effects between electrical, mechanical and magnetic responses.

2. Computational details

The first-principle calculations are based on spin-polarized density functional theory using projector-augmented wave methods[34] as implemented in the Vienna *ab initio* simulation package (VASP).[35–37] Exchange–correlation interactions are described in the generalized gradient approximation (GGA)[38] within the Perdew–Burke–Ernzerhof (PBE).[39] Plane waves with a kinetic energy cutoff of 600 eV are used to expand the valance electron ($2s^2 2p^1$ for B, $2s^2 2p^3$ for N) wavefunctions. A vacuum spacing of 15 Å is used to avoid the interactions between the layers. The Brillouin zone is sampled by a $7 \times 7 \times 1$ k-point grid within the Monkhorst–Pack scheme[40] for our calculations, which ensures that the total energy convergence is within 0.01% difference with respect to the number of k points. For geometry relaxation, the total energy change and the force on each atom are less than 10^{-5} eV and 10^{-3} eV/Å, respectively. The elastic tensor coefficients (C_{ijkl}) are calculated by using the finite difference method[41] and the strain coefficients of the piezoelectric tensor (e_{ijk}) are calculated by using density-functional perturbation theory (DFPT).[41]

3. Results and discussion

3.1. Structural and stable properties

Following the idea that the h-BN monolayer is decorated by the triangle-shaped vacancy, we discuss the two configuration systems as shown in Fig. 1. Compared with the pristine h-BN sheet, the h-BN with boron vacancies (marked as V_B-BN) consists of those vacancies each of which is due to the missing of one boron atom in primitive cell as shown in Fig. 1(a). As a result, in view of the overall sheet, this forms a regular spaced triangle-shaped vacancy. The three doubly coordinated nitrogen atoms are the closest ones to the vacancy. For convenience of discussion, we here denote the trebly coordinated and the doubly coordinated N atoms as N1 and N2, respectively. The unit cell of the V_B-BN contains seven atoms as denoted by black dashed lines in Fig. 1(a) in which the B-to-N ratio is 3 : 4. The optimized lattice constant is $a = 4.975$ Å. The B–N1 (1.403 Å) and B–N2 (1.408 Å) bond lengths of the V_B-BN are less than the B–N (1.45 Å) bond length of the pristine h-BN sheet. This fact indicates that the interactions between the B and N atoms of the V_B-BN are stronger than that of the pristine h-BN. Here, we perform a Bader charge analysis for better elucidating the effective charges at the B and N atoms. The different outer shell electronic configurations and electronegativities of atoms cause an imbalance of electric charges within the B−N bond. Consequently, the electrons are shared unevenly, forming a polar covalent bond. A positive number denoted by "+" means that this atom loses electrons and has a positive charge, and similarly, a negative number denoted by "−" means that this atom obtains electrons and has a negative charge. As listed in Fig. 1(a), Bader analysis reveals that there are certain electronic charge transfers from the less electronegative B atoms to the more electronegative N atoms, which is the same as the pristine h-BN. In the unit cell of the V_B-BN, about $2.18|e|$ charge is transferred to the N1 and N2 atoms from each B atom. Each N1 atom obtain $2.15|e|$ while the N2 atom gains less charge ($1.46 \pm 0.01|e|$).

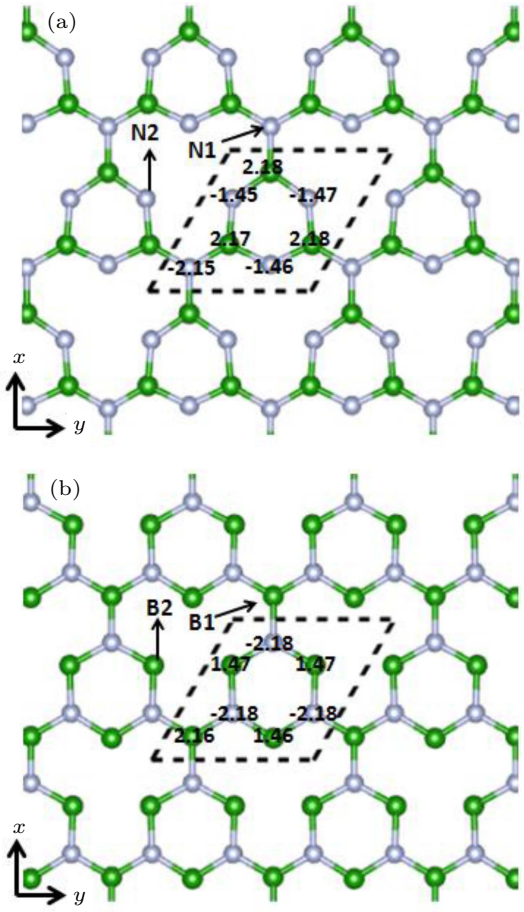


Fig. 1. (color online) Optimized structures of (a) boron vacancy V_B-BN and (b) nitrogen vacancy V_N-BN. Gray and green spheres represent nitrogen and boron atoms, respectively. Rhombus marked by black dashed lines denotes primitive cell.

Figure 1(b) displays the structure model of the h-BN with nitrogen vacancies (denoted as V_N-BN). Like the V_B-BN defect case, the V_N-BN defect loses one nitrogen atom in the

unit cell compared with the pristine h-BN sheet as shown in Fig. 1(b). In contrast to the V_B-BN, it is clear that the nitrogen vacancy is surrounded by the three doubly coordinated B atoms. Geometrical relaxation of the V_N-BN is performed by considering the rhombic primitive cell as denoted by black dashed lines in Fig. 1(b). Here, we group the trebly coordinated and the doubly coordinated B atoms as B1 and B2, respectively. The optimized lattice constant of the V_N-BN is found to be $a = 4.940$ Å, which is smaller than that of the V_B-BN. In the unit cell of the V_N-BN, the ratio between the numbers of atoms B and N is 4:3. The B1–N bond length is 1.419 Å which is slightly larger than the B–N1 (1.403 Å) bond length of the V_B-BN, while B2-N bond length is 1.456 Å which is close to the B–N (1.450 Å) bond length of the pristine h-BN sheet. Therefore, it seems that the V_B-BN is easier to form than the V_N-BN. The Bader charge analysis demonstrates that each N atom gains $2.18|e|$ from the neighboring B atoms. The B1 atom transfers $2.16|e|$ to the neighboring N atoms, but the B2 atom transfers 1.47 or $1.46|e|$ to the neighboring N atoms.

3.2. Electronic and magnetic properties

Figure 2(a) shows the spin-polarized band structure and total density of states (TDOS) for the V_B-BN system. We find that the bands of the spin-down electron states exceed slightly those of the spin-up electron states below an energy of 2 eV in the spin-polarized band structure, inducing a spontaneous polarization which is in accordance with the TDOS of this system. Unlike the semiconducting property of pristine h-BN sheet, this V_B-BN system displays metallic behavior, which originates from the pseudodangling bonds of N atoms neighboring with B atom vacancy. Whether its state is a spin-up state or spin-down state, the valence band crosses the Fermi level between all high symmetry points, spreading the whole Brillouin zone. According to the partial density of states (PDOS) in Fig. 2(b), we further shows that the magnetic property is mainly contributed by unsaturated 2p orbital electrons of N2 atoms, which is consistent with the results of 3D spin charge density distribution in Fig. 2(d).

Three-dimensional (3D) plots of spin charge density distributions of the V_B-BN in Fig. 2(d) visualize the magnetic property clearly. The 3D spin charge density distribution $[\Delta\rho(r) = \rho_\uparrow(r) - \rho_\downarrow(r)]$ reveals that the magnetic moments are mainly localized on N2 atoms and secondarily localized on N1. The total magnetic moment is $0.46\mu_B$ per cell. The N1 and N2 atoms contribute an atomic moment of $0.059\mu_B$, $0.100\mu_B$, respectively. Compared with N1 and N2 atoms, each B atom carry very small magnetic moment $(-0.011\mu_B)$. In order to understand the chemical bonding of the V_B-BN system,

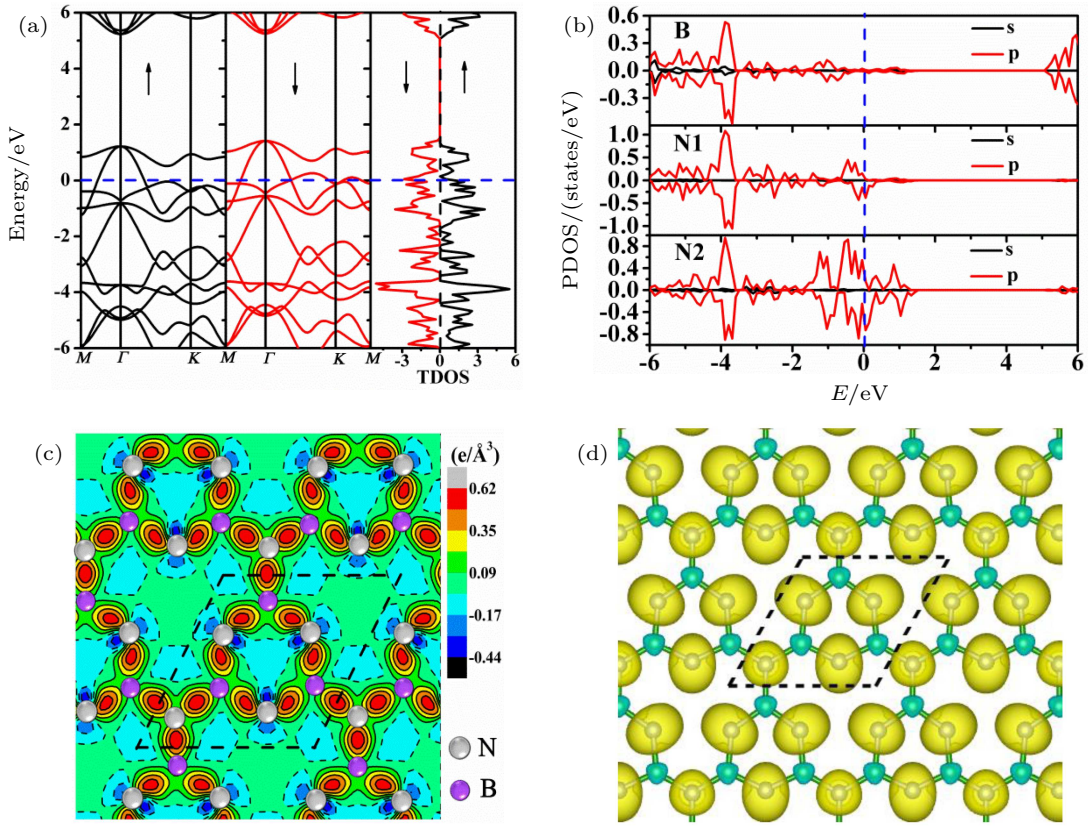


Fig. 2. (color online) ((a), (b)) Spin-polarized band structures with a Fermi level sets at zero energy, total density of states (TDOS) and partial density of states (PDOS) of the V_B-BN. (c) 2D plot of charge density difference of V_B-BN. (d) 3D plot of spin charge density distribution of the V_B-BN atan isovalue of 0.004 e/Å^3.

we draw its 2D plots of the charge density difference (defined as the total charge density minus the contributions of isolated B and N atoms) in Fig. 2(c). A positive value (solid contour line) indicates an increase in electron density, and a negative value (dashed contour line) means the electron density loss with respect to the superposition of the atomic electron density. Figure 2(c) shows that there is electronic charge accumulation in the middle of the bond between the neighboring B and N atoms, which indicates how the B–N covalent bonds are formed. There is electronic charge depletion around the N2 atoms. Because each nitrogen atom has a valence configuration of $2s^2 2p^3$, two electrons of the N2 atom participate in the covalent bond with the boron atoms, two electrons of the N2 atom make up a lone pair electron, and the remaining one electron is shared between pseudodangling sp^3 bond which leads each N2 atom to own a magnetic moment. Because three electrons of the N1 atom participate in the covalent bond with the boron atoms, there is no electron to be shared between pseudodangling sp^3 bonds for the N1 atom. However, the shared electron of N2 atom has an influence on the homologous N1 atom and thus causes the N1 atom to have a small magnetic moment.

The spin-polarized band structure and total density of states (TDOS) of the V_N-BN are plotted in Fig. 3(a). In the spin-polarized band structure, the spin-up and spin-down states have different dispersions. The bands with energy lower than −4 eV are fully occupied and thus contribute little to spin polarization. However, the flat band near Fermi energy is split into two branches. The spin-up branch is occupied and the spin-down branch is empty, leading to a spontaneous polarization with a total magnetic moment of $1.0\mu_B$ per cell, for which the B1 and B2 atoms contribute atomic moments of $0.072\mu_B$ and $0.132\mu_B$, respectively. Comparing with the V_B-BN, the magnetic moment of the V_N-BN is about twice larger than that of the V_B-BN, but the leading role in their magnetism is played by these doubly coordinated atoms surrounding the vacancy for both V_B-BN and V_N-BN systems. Interestingly, the V_N-BN presents a half-metallic characteristic where spin-down state remains as an indirect band-gap insulator with a band gap of about 4.2 eV, which is smaller than 4.68 eV for h-BN by 0.48 eV.[26] The spin-up state is metallic as shown in the spin-polarized band structure. The result is in accordance with the calculated TDOS. In the spin-down state, the TDOS is zero at the Fermi level with an energy gap of 4.2 eV, while there is a finite TDOS at the Fermi level in the spin-up state, revealing half-metallic behavior in the V_N-BN system. Thus, the V_N-BN is only conductive to the spin-up electrons, which leads to a 100% spin polarization. The corresponding spin charge density distribution with an isosurface of 0.01 e/Å^3 is depicted in Fig. 3(d), which shows that the spin states at different atoms have different spin orientations and the magnetism is mainly contributed by the B atoms. The 2D plots of the charge density difference of the V_N-BN system in Fig. 3(c)

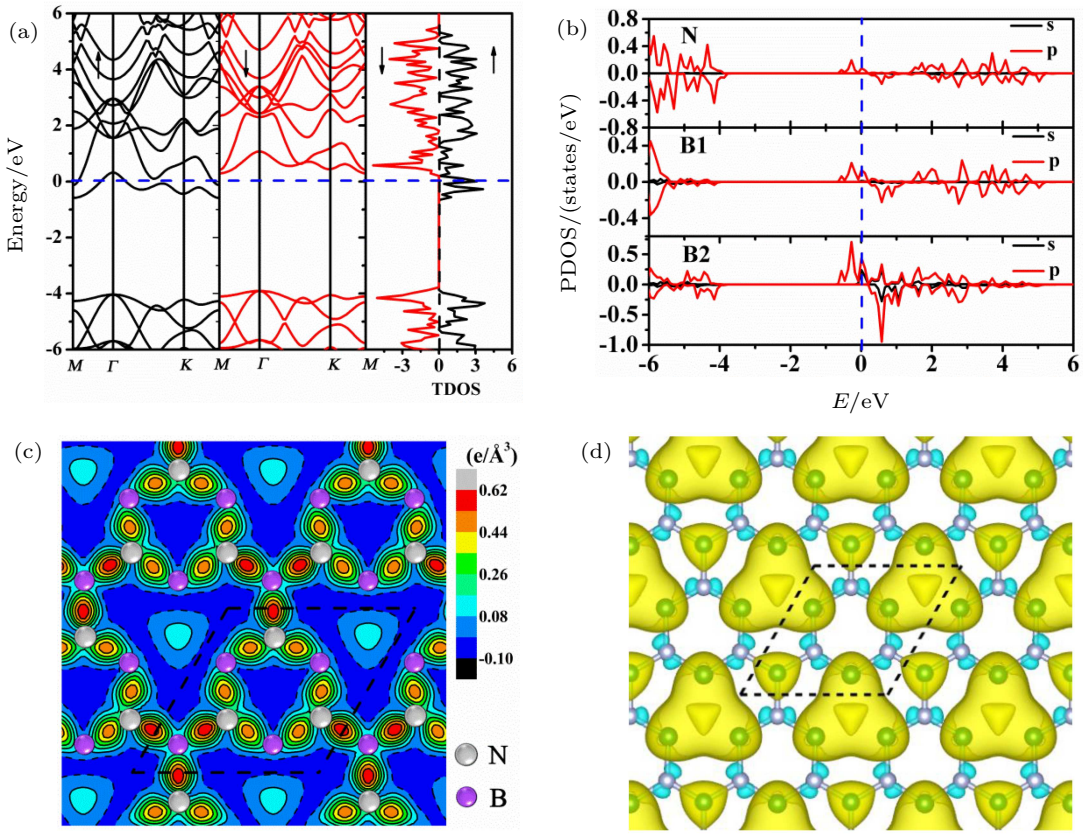


Fig. 3. (color online) The legend is similar to that in Fig. 2 while the results in panels (a)–(d) are for the V_N-BN. (d) Yellow and light blue indicate the spin-up and spin-down states, respectively, in the isosurface 0.01 e/Å^3.

depicts the nature of the chemical bonding. Figure 3(c) shows that the B atom surrounded by three triangular N vacancies has stronger interaction with neighboring N atoms than other B atoms. This fact can contribute to the stability of the V_N-BN structure. As is well known, B atom has a valence configuration of $2s^2 2p^1$, once one nitrogen atom is removed, each B2 atom will remain one unpaired electron. Therefore the unpaired electrons form pseudodangling bond at the position of vacancy and the B2 atoms will produce exactly identical magnetic moment. Like N1 atom in the V_B-BN, the B1 atom in V_N-BN has a little magnetic moment which is affected by B2 atoms. The point is demonstrated by the calculated partial density of states in Fig. 3(b) again, which are mainly dominated by 2p states of B2 atom at the Fermi level.

3.3. Mechanical and piezoelectric properties

In preceding discuss, we find the V_B-BN to be metallic and hence not piezoelectric. Then we perform the piezoelectric effect calculation on V_N-BN system. Adopting these optimized structures, we can calculate the elastic constants and piezoelectric coefficients of the pristine and N atom vacancy-decorated h-BN. The elastic constants reflect the stress–strain relation of material, which is defined as

$$\sigma_i = C_{ij}\varepsilon_j, \tag{1}$$

where σ and ε are the stress and strain tensor, respectively, and C_{ij} are the elastic constants.

Similarly, the piezoelectric coefficients can be expressed as

$$e_{ijk} = \frac{\partial P_i}{\partial \varepsilon_{jk}}, \tag{2}$$

$$d_{ijk} = \frac{\partial P_i}{\partial \sigma_{jk}}, \tag{3}$$

where both the piezoelectric stress coefficients e_{ijk} and the piezoelectric strain coefficients d_{ijk} are third-rank tensors, relating the polarizations P_i to strain ε_{jk} and stress σ_{jk}, respectively.

We know that the performing of symmetry analysis on the elastic and piezoelectric tensors can further reduce the number of independent tensor coefficients by using the point group of the 2D material. There are many regular triangle-shaped holes in vacancy-decorated h-BN. However, compared with the pristine h-BN, the vacancy-decorated h-BN still belongs to the D_{3h} ($6\bar{m}2$) point group. Employing the standard Voigt notation, i.e., 1-*xx*, 2-*yy*, 3-*zz*, 4-*yz*, 5-*xz*, 6-*xy*, the elastic and piezoelectric coefficients can become

$$C_{ij} = \begin{Bmatrix} C_{11} & C_{12} & 0 \\ C_{12} & C_{11} & 0 \\ 0 & 0 & \frac{C_{11}-C_{12}}{2} \end{Bmatrix}, \tag{4}$$

$$e_{ij} = \begin{Bmatrix} e_{11} & -e_{11} & 0 \\ 0 & 0 & -e_{11} \end{Bmatrix}, \tag{5}$$

$$d_{ij} = \begin{Bmatrix} d_{11} & -d_{11} & 0 \\ 0 & 0 & -d_{11} \end{Bmatrix}, \tag{6}$$

where we can conclude that the only unique piezoelectric coefficients are e_{11} and d_{11}. In addition, the corresponding piezoelectric strain coefficients d_{11} are further obtained from the inversion of the transformation relationship as follows:

$$d_{11} = \frac{e_{11}}{C_{11} - C_{12}}. \tag{7}$$

The elastic constants and piezoelectric coefficients calculated for the pristine h-BN and the V_N-BN are listed in Table 1. In the present study, the elastic constants and piezoelectric coefficients of the pristine h-BN sheet are calculated to be $C_{11} = 289$ N/m and $C_{12} = 64$ N/m by using the finite differences method and $e_{11} = 1.40 \times 10^{-10}$ C/m and $d_{11} = 0.62$ pm/V by using density-functional perturbation theory (DFPT), which are well consistent with previous results of $C_{11} = 291$ N/m, $C_{12} = 62$ N/m, $e_{11} = 1.3810^{-10}$ C/m, and $d_{11} = 0.60$ pm/V by Duerloo *et al.*[26] Obviously, the elastic constants of the V_N-BN become smaller than those of the pristine counterpart. Comparing the C_{11} of the V_N-BN with that of the pristine h-BN, we find that the elastic constant 289 N/m of the pristine h-BN is much larger than triple the elastic constant (86 N/m) of the V_N-BN, indicating that the induced N atom vacancies make it more flexible. As can be seen from Table 1, the calculated piezoelectric stress coefficients e_{11} of the V_N-BN monolayer are of the same order of magnitude as other popular piezoelectric materials listed for comparison. The V_N-BN exhibits a greater piezoelectric response than the pristine h-BN It is seen that the piezoelectric stress coefficient e_{11} of V_N-BN (2.36×10^{-10} C/m) is much larger than that of the pristine BN monolayer (1.40×10^{-10} C/m). It is worth noting that the piezoelectric stress coefficient e_{11} of V_N-BN is larger than 1.5 times that of pristine h-BN, larger than the maximum one predicted for F- and H-doped h-BN in a chair conformation.[31] Furthermore, the piezoelectric stress coefficient e_{11} of V_N-BN is larger than those of 2*H*-$NbSe_2$ (2.22×10^{-10} C/m) and 2*H*-$NbTe_2$ (1.84×10^{-10} C/m). The calculated piezoelectric strain coefficient d_{11} of V_N-BN (12.42 pm/V) is one order of magnitude higher than those of all the other materials listed in Table 1, and it is 20 times larger than that of pristine h-BN and also 1 order of magnitude higher than the values for the h-MoS_2, 2H-$NbSe_2$ and 2H-$NbTe_2$ monolayer. Figure 3(a) shows that the spin-up state of the V_N-BN presents metallic characteristic, and the spin-down state of the V_N-BN remains an indirect band-gap insulator with a band gap of about 4.2 eV. The piezoelectric coefficient is mainly due to the electronic structure of spin-down electronic states in the V_N-BN system. The regularly triangular vacancies do not change the symmetry

of the h-BN sheet when the symmetric center is located at the atom in the lower-left corner of the unit cell. Then the V_N-BN still belongs to the D_{3h} ($6\overline{m}2$) point group. However, the non-centrosymmetric triangular vacancy will strengthen the polarized degree of this sheet. That is why the piezoelectric stress coefficients e_{11} of the V_N-BN is larger than that of the pristine h-BN sheet. We can deduce that other structures like the h-BN with losing one atom to form triangular vacancy in the unit cell could make larger piezoelectric response. Moreover, the pristine h-BN and MoS_2 monolayer lose their piezoelectric effect when even-numbered layers are present, but the piezoelectricities of these h-BN monolayers riddled with regularly spaced triangular holes, which are studied here and listed in Table 1, can be retained if they are stacked like g-C_3N_4 based on a similar mechanism.[32]

Table 1. Calculated elastic constants (C_{ij}) and piezoelectric coefficients (e_{ij} and d_{ij}) of the pristine and V_N-BN. Other experimental and theoretical values of popular 2D piezoelectric materials are listed for comparison. Elastic constants (C_{ij}) are in units of N/m, piezoelectric stress coefficients (e_{ij}) in 10^{-10} C/m for 2D system, and piezoelectric strain coefficients (d_{ij}) in pm/V.

System	C_{11}	C_{12}	e_{11}	d_{11}
h-BN[26]	291	62	1.38	0.60
h-BN	289	64	1.40	0.62
V_N-BN	86	67	2.36	12.42
h-BN + F,H (chair)[31]			1.81	1.27
2H-$NbSe_2$[42]			2.22	3.87
2H-$NbTe_2$[42]			1.84	4.45
h-MoS_2 (cal.)[26]			3.64	3.73
h-MoS_2 (exp.)[43]			2.9	

4. Conclusions

In this work, we investigate the magnetic and piezoelectric properties of hexagonal boron nitride (h-BN) monolayer riddled with regularly spaced triangular holes by using first-principle calculations. It is found that the triangular holes can indeed induce spontaneous magnetizations in the V_B-BN and V_N-BN systems. More interestingly, the band structure of V_N-BN indicates that the V_N-BN has the desired half-metallic behavior. As for piezoelectricity, the piezoelectric strain coefficients d_{11} (12.42 pm/V) of the V_N-BN is also 20 times larger than that of pristine h-BN and one order of magnitude higher than the value of the h-MoS_2 monolayer. The spin-down electronic states mainly contribute to the higher piezoelectric coefficient in the V_N-BN system. It is worth noting that the V_N-BN system riddled with different regularly spaced triangular holes has no center of inversion symmetry and may not lose piezoelectricity when even-numbered layers are present. Our study demonstrates that the triangle-shaped vacancy is used to tailor the magnetic and piezoelectric properties of h-BN monolayer. The co-existence of piezoelectricity and magnetism in h-BN with triangle-shaped vacancy means promising performance for potential applications in the integration of magnetic and electromechanical nano-devices.

References

[1] Novoselov K S, Geim A K, Morozov S V, Jiang D, Zhang Y, Dubonos S V, Grigorieva I V and Firsov A A 2004 *Science* **306** 666
[2] Watanabe K, Taniguchi T and Kanda H 2004 *Nat. Mater.* **3** 404
[3] Novoselov K, Jiang D, Schedin F, Booth T, Khotkevich V, Morozov S and Geim A 2005 *Proc. Natl. Acad. Sci. USA* **102** 10451
[4] Degheidy A R and Elkenany E B 2017 *Chin. Phys. B* **26** 086103
[5] Han W Q, Wu L, Zhu Y, Watanabe K and Taniguchi T 2008 *Appl. Phys. Lett.* **93** 223103
[6] Nag A, Raidongia K, Hembram K P, Datta R, Waghmare U V and Rao C 2010 *ACS Nano* **4** 1539
[7] Zhi C, Bando Y, Tang C, Kuwahara H and Golberg D 2009 *Adv. Mater.* **21** 2889
[8] Jasuja K 2011 *Designing Nanoscale Constructs from Atomic Thin Sheets of Graphene, Boron Nitride and Gold Nanoparticles for Advanced Material Applications* (Kansas State University)
[9] Zhao L S, Wang Y, Chen C P, Liu L L, Yu H X, Zhang Y, Chen Y and Wang X C 2017 *Physica E* **91** 82
[10] Liu L L, Chen C P, Zhao L S, Wang Y and Wang X C 2017 *Carbon* **115** 773
[11] Chen X, Xu L, Liu L L, Zhao L S, Chen C P, Zhang Y and Wang X C 2017 *Appl. Surf. Sci.* **396** 1020
[12] Jin C, Lin F, Suenaga K and Iijima S 2009 *Phys. Rev. Lett.* **102** 195505
[13] Azevedo S, Kaschny J R, de Castilho C M C and de Brito Mota F 2009 *The European Physical Journal B* **67** 507
[14] Azevedo S, Kaschny J R, de Castilho C M and de Brito Mota F 2007 *Nanotechnology* **18** 495707
[15] Lin Y, Williams T V, Cao W, Elsayed-Ali H E and Connell J W 2010 *The Journal of Physical Chemistry C* **114** 17434
[16] Noorizadeh S and Shakerzadeh E 2012 *Computational Materials Science* **56** 122
[17] Lvova N and Ananina O Y 2016 *Comput. Mater. Sci.* **115** 11
[18] Zhou J, Wang Q, Sun Q and Jena P 2010 *Phys. Rev. B* **81** 085442
[19] Yin J, Li J, Hang Y, Yu J, Tai G, Li X, Zhang Z and Guo W 2016 *Small* **12** 2942
[20] Wang Y and Ding Y 2014 *J. Phys.: Condens. Matt.* **26** 43
[21] Si M S and Xue D S 2007 *Phys. Rev. B* **75** 193409
[22] Ekinci K and Roukes M 2005 *Rev. Sci. Instrum* **76** 061101
[23] Huang X M H, Zorman C A, Mehregany M and Roukes M L 2003 *Nature* **421** 496
[24] Sai N and Mele E 2003 *Phys. Rev. B* **68** 241405
[25] Reed E J 2015 *Nat. Nanotechnology* **10** 106
[26] Duerloo K A N, Ong M T and Reed E J 2012 *The Journal of Physical Chemistry Letters* **3** 2871
[27] Michel K and Verberck B 2009 *Phys. Rev. B* **80** 224301
[28] Li W and Li J 2015 *Nano Research* **8** 3796
[29] Wang J L and Hu W D 2017 *Chin. Phys. B* **26** 037106
[30] Ding Y and Wang Y 2016 *J. Mater. Chem. C* **4** 1517
[31] Noor-A-Alam M, Kim H J and Shin Y H 2014 *Phys. Chem. Chem. Phys.* **16** 6575
[32] Zelisko M, Hanlumyuang Y, Yang S, Liu Y, Lei C, Li J, Ajayan P M and Sharma P 2014 *Nat. Commun.* **5** 4284
[33] Yang J, Kim D, Hong J and Qian X 2010 *Surf. Sci.* **604** 1603
[34] Blöchl P E 1994 *Phys. Rev. B* **50** 17953
[35] Kresse G and Hafner J 1994 *Phys. Rev. B* **49** 14251
[36] Kresse G and Furthmüller J 1996 *Phys. Rev. B* **54** 11169
[37] Kresse G and Furthmüller J 1996 *Comput. Mater. Sci.* **6** 15
[38] Perdew J P, Chevary J A, Vosko S H, Jackson K A, Pederson M R, Singh D J and Fiolhais C 1992 *Phys. Rev. B* **46** 6671
[39] Perdew J P, Burke K and Ernzerhof M 1996 *Phys. Rev. Lett.* **77** 3865
[40] Monkhorst H J and Pack J D 1976 *Phys. Rev. B* **13** 5188
[41] Wu X, Vanderbilt D and Hamann D 2005 *Phys. Rev. B* **72** 035105
[42] Blonsky M N, Zhuang H L, Singh A K and Hennig R G 2015 *ACS Nano* **9** 9885
[43] Zhu H Y, Wang Y, Xiao J, Liu M, Xiong S M, Wong Z J, Ye Z L, Ye Y, Yin X B and Zhang X 2015 *Nat. Nanotechnol.* **10** 151